Journal Pre-proofs

Nanoparticle tracking analysis and statistical mixture distribution analysis to quantify nanoparticle—vesicle binding

Isabel U. Foreman-Ortiz, Ting Fung Ma, Brandon M. Hoover, Meng Wu, Catherine J. Murphy, Regina M. Murphy, Joel A. Pedersen

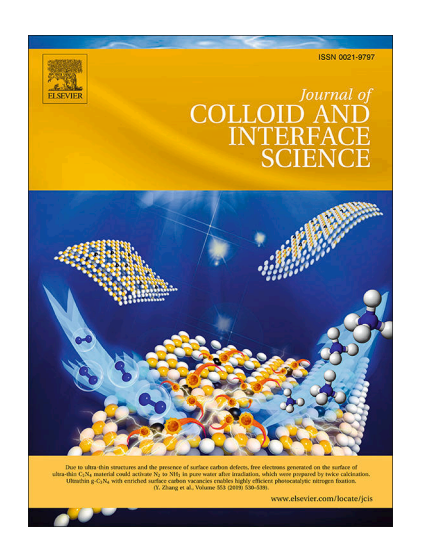
PII: S0021-9797(22)00159-X

DOI: https://doi.org/10.1016/j.jcis.2022.01.141

Reference: YJCIS 29677

To appear in: Journal of Colloid and Interface Science

Received Date: 21 April 2021 Revised Date: 16 January 2022 Accepted Date: 22 January 2022



Please cite this article as: I.U. Foreman-Ortiz, T. Fung Ma, B.M. Hoover, M. Wu, C.J. Murphy, R.M. Murphy, J.A. Pedersen, Nanoparticle tracking analysis and statistical mixture distribution analysis to quantify nanoparticle–vesicle binding, *Journal of Colloid and Interface Science* (2022), doi: https://doi.org/10.1016/j.jcis. 2022.01.141

This is a PDF file of an article that has undergone enhancements after acceptance, such as the addition of a cover page and metadata, and formatting for readability, but it is not yet the definitive version of record. This version will undergo additional copyediting, typesetting and review before it is published in its final form, but we are providing this version to give early visibility of the article. Please note that, during the production process, errors may be discovered which could affect the content, and all legal disclaimers that apply to the journal pertain.

© 2022 Published by Elsevier Inc.

Journal Pre-proofs

Nanoparticle tracking analysis and statistical mixture distribution analysis to quantify nanoparticle—vesicle binding

Isabel U. Foreman-Ortiz,[†] Ting Fung Ma,[‡] Brandon M. Hoover,[¶] Meng Wu,[□] Catherine J. Murphy,^{□*} Regina M. Murphy,[¶] Joel A. Pedersen,^{†,Δ}

CRediT authorship contribution statement

Isabel U. Foreman-Ortiz: Conceptualization, Methodology, Formal Analysis, Investigation, Writing - original draft, Visualization. Ting Fung Ma: Methodology, Software, Formal Analysis, Writing - original draft. Brandon M. Hoover: Investigation, Writing - original draft. Meng Wu: Resources, Writing - original draft. Catherine J. Murphy: Resources, Reviewed manuscript. Writing - Review and editing manuscript. Regina M. Murphy: Methodology, Resources, Reviewed manuscript. Joel A. Pedersen: Conceptualization, Writing - Review & editing manuscript, Supervision.

Corresponding Author

*E-mail: <u>murphycj@illinois.edu</u>. Tel (01) 217-333-7680, fax (01) 217-244-3186

ORCID

Joel A. Pedersen: 0000-0002-3918-1860 Regina Murphy: 0000-0002-6196-5450

Isabel U. Foreman-Ortiz: 0000-0003-3169-7026

Ting Fung Ma: 0000-0001-6028-5640 Brandon Hoover: 0000-0002-4511-0217 Catherine J. Murphy: 0000-0001-7066-5575

[†] Department of Chemistry, University of Wisconsin, Madison, WI 53706

[‡] Department of Statistics, University of Wisconsin, Madison, WI 53706

[¶] Department of Chemical and Biological Engineering, University of Wisconsin, Madison, WI 53706

 [□] Department of Chemistry, University of Illinois at Urbana-Champaign, Urbana, IL 61801
△ Departments of Soil Science and Civil & Environmental Engineering, University of Wisconsin, Madison, WI 53706

ABSTRACT

Nanoparticle tracking analysis (NTA) is a single particle tracking technique that in principle provides a more direct measure of particle size distribution compared to dynamic light scattering (DLS). Here, we demonstrate how statistical mixture distribution analysis can be used in combination with NTA to quantitatively characterize the amount and extent of particle binding in a mixture of nanomaterials. The combined approach is used to study the binding of gold nanoparticles to two types of phospholipid vesicles, those containing and lacking the model ion channel peptide gramicidin A. This model system serves as both a proof of concept for the method and a demonstration of the utility of the approach in studying nano-bio interactions. Two diffusional models (Stokes–Einstein and Kirkwood–Riseman) were compared in the determination of particle size, extent of binding, and nanoparticle:vesicle binding ratios for each vesicle type. The combination of NTA and statistical mixture distributions is shown to be a useful method for quantitative assessment of the extent of binding between particles and determination of binding ratios.

1. Introduction

Nanoparticle tracking analysis (NTA) is a single-particle tracking technique that allows high-resolution determination of particle size distributions for polydisperse samples [1]. In NTA, the Brownian motion of individual particles diffusing in solution is tracked under laser illumination using a microscope equipped with a video camera [1]. The mean squared displacement in the x–y plane is used to calculate translational diffusion coefficients (D_T) for individual particles, yielding a number distribution of diffusivities, from which hydrodynamic diameters (d_h) can be derived by the Stokes–Einstein or other diffusional models [1,2]. The determination of a true number distribution of diffusion coefficients represents a distinct advantage over ensemble techniques such

as dynamic light scattering (DLS) [1]. The upper bound for the size of particles amenable to tracking by NTA is ~1000 nm, whereas the lower size limit depends on particle refractive index, laser wavelength and power, and sensitivity of the camera, and can range from ~10 to ~50 nm [3–5].

NTA has been used to characterize the hydrodynamic properties of nanoscale particles (e.g., engineered nanoparticles, liposomes, extracellular vesicles, viruses, protein aggregates) [3– 8] and to monitor protein aggregation [9]. Specifically related to this work, NTA has been used to monitor the bioconjugation of gold nanoparticles (AuNPs) by protein A and subsequent interaction of immunoglobulin G (IgG) with the conjugated particles by measuring the change in mean hydrodynamic diameter as function of protein A or IgG concentration [1,3,7]. In polydisperse mixtures in which particles may bind to one another such as in the aforementioned study, it would be particularly illuminating to not only compare mean particle sizes but also to deduce the proportion of particles in each binding state (e.g., unbound, pairs, triplets). Since NTA creates a size distribution from particle-by-particle measurements, the technique has the potential to achieve accurate determination of particle binding-state distribution in polydisperse samples [3–5]. Approaches need to be developed to analyze NTA data from the highly polydisperse samples that result from mixtures containing both unbound and (multiply) bound populations. This challenge can be met by application of statistical mixture distribution analysis to histograms of particle diffusivities determined by NTA. Mixture distribution analysis can also provide an estimate of binding ratios between particle types present in a mixture.

The objective of this study was to evaluate the application of statistical mixture distribution analysis to NTA data for the purpose of estimating bound populations in a polydisperse mixture. The experimental system investigated consisted of small unilamellar vesicles (SUVs) and anionic

gold nanoparticles (AuNPs). SUVs are commonly used to investigate the interaction of nanoparticles with phospholipid bilayers as simple models for cell membranes [10–13]. Understanding of nanoparticle interaction with cell membranes can aid the design of nanoparticles for biomedical applications[14–16] and inform the assessment of potential adverse outcomes of exposures to nanoparticles due to their release into the environment [13,14,17–20]. Other work in the literature finds multiple stoichiometries and binding modes of AuNPs with liposomes by many complementary techniques, including fluorescence correlation spectroscopy, x-ray scattering, and cryo-electron microscopy; in most cases, it is found that multiple small AuNPs bind to large liposomes.[21–23] In the present study, we employed vesicles composed of zwitterionic lipids, and compared AuNP binding to vesicles versus vesicles containing the model ion channel protein gramicidin A (gA); in our case, the effective size of the AuNPs were of similar size to the vesicles. The motivation for choosing this experimental system came from prior work that demonstrated that anionic AuNP binding to zwitterionic lipid bilayers can modulate gA activity [24]. In the mixture distribution analysis we evaluated two models of particle shape (Stokes-Einstein and Kirkwood–Riseman) using the statistical fitness of each model to determine model suitability. We demonstrate that the combination of NTA and mixture distribution analysis can be used to discriminate nanoparticle binding to different vesicle types – here, either lacking or containing gA. Thus, the approach developed can be used to investigate the influence of individual membrane components on nanoparticle binding. This method provides a unique advantages over ensemble techniques such as dynamic light scattering (DLS) for assessment of particle–particle interactions that arise in complex colloidal systems such as nanoparticle—vesicle mixtures.

2. Materials and methods

2.1. Synthesis and characterization of gold nanoparticles

2.1.1. Materials

We obtained 3-mercaptopropionoic acid (MPA), gold(III) chloride trihydrate (HAuCl₄·3H₂O), and sodium hydroxide from Sigma Aldrich. Sodium borohydride was purchased from Fluka. We procured 1,2-diphytanoyl-*sn*-glycero-3-phosphocholine (DPhPC; 4ME 16:0 PC) in chloroform from Avanti Polar Lipids (Alabaster, AL), and gramicidin A (gA) from Sigma Aldrich. We acquired 4-(2-hydroxyethyl)-1-piperazineethanesulfonic acid (HEPES) from Dot Scientific. All chemicals were the highest purity ones available from each vendor.

2.1.2. Synthesis of gold nanoparticles capped with 3-mercaptopropionic acid (MPA)

We synthesized nominal 3 nm diameter MPA-AuNPs (hereafter referred to only as AuNPs) following a published protocol with modifications [25]. Briefly, we added HAuCl₄ (3 mL, 0.1 M) to 700 mL ultrapure water in an Erlenmeyer flask. Subsequently, 333 μ L of 0.1 M MPA followed by 1.4 mL of 1.0 M NaOH solution was added to the aqueous solution under gentle stirring. Fresh 0.1 M NaBH₄ solution (10 mL) was quickly added to the above reaction mixture under rigorous stirring. The combined solutions rapidly changed color to a deep red-brown, and the reaction mixture was stirred gently for 2 h. The AuNPs were purified by centrifugation (55 min, 13,000g, twice) and redispersed in 1 mM NaOH after the first centrifugation and ultrapure water (\geq 18 M Ω ·cm) after the second centrifugation.

2.1.3. *Ultraviolet-visible absorbance spectroscopy*

The UV-vis spectra of AuNP suspensions were acquired on a Cary 5000 UV-vis spectrophotometer. The normalized UV-vis spectrum of AuNPs is shown in Fig. S1. The diameter of AuNP was estimated in solution by UV-vis spectroscopy to be around 3.3 nm [26]. TEM image analysis indicated that the core diameter of AuNPs was 3.3 ± 0.6 nm (n > 200).

2.1.4. Transmission electron microscopy (TEM)

For TEM imaging, 5 µL of a dilute solution of AuNPs was drop-cast onto a copper TEM grid with 400 mesh ultrathin carbon film on lacey carbon support film (Ted Pella), and images were acquired with a JEOL 2100 cryo TEM. A representative TEM image is shown in Fig. S1. The TEM sizing analysis was performed by ImageJ.

2.2. Formation and characterization of SUVs.

Small unilamellar vesicles were formed using the extrusion method [27,28]. We chose to construct vesicles from the zwitterionic phospholipid DPhPC to allow comparison to previous studies where gA ion channels were embedded in suspended planar DPhPC membranes [24]. Briefly, DPhPC lipids purchased in chloroform and gA diluted in 2,2,2-trifluoroethanol were combined to a DPhPC:gA molar ratio of about 27.8:1. The mixture was then completely dried under ultrapure N₂ gas, followed by rehydration to a lipid concentration of 2.5 mM in 0.150 M KCl buffered to pH 7.5 using 0.01 M HEPES by sonication for 30 min. The salt concentration was chosen for both physiological relevance in terms of ionic strength, and direct comparison to a previous study indicating that AuNPs can alter the function of gA [24]. The resulting solution of lipid and gA was then extruded 11 times through a 0.05 µm polycarbonate filter (Whatman). Vesicles lacking gA were formed in a similar manner with DPhPC lipid only. All vesicle solutions were used within 1 week of extrusion and were stored at 4 °C.

2.3. Fluorescence spectroscopy

Fluorescence spectroscopy was used to confirm the presence of gA in vesicles by observation of an emission maximum at 328 nm when referenced to vesicles lacking gA [29,30]. This peak indicates the presence of gA in its ion channel conformation, which occurs only when

embedded in the lipid membrane [29,30]. Fluorescence spectra were measured using an ISS K2 spectrofluorimeter set to 1.0 mm slit width and equipped with a neutral density filter of 1.0 optical density. An excitation wavelength of 280 nm was used, and emission was collected from 300 to 400 nm. Fig. S2 depicts the presence of a maxima at 328 nm, indicating the presence of gA in vesicles.

2.4. Hydrodynamic and electrokinetic properties of nanoparticles and SUVs

2.4.1. Nanoparticle tracking analysis (NTA)

Binding of gold nanoparticles to vesicles consisting of DPhPC with (SUV-gA) and without (SUV) the gA peptide was monitored by NTA. Briefly, particles in the sample scatter light from a 405 nm laser, and the scattered light is tracked using a high-sensitivity camera. By measuring the trajectory of the diffusing particle over a tracking time t, the translational diffusion coefficient D_T is calculated [4,31]:

$$\overline{(x,y)^2} = 4D_{\mathrm{T}}t\tag{1}$$

where $k_{\rm B}$ is the Boltzmann constant.

All NTA measurements were performed with a Nanosight LM10 (Nanosight) using a 405 nm laser at room temperature. Samples were prepared by combining vesicles at 2.5 mM lipid with 0.05 μL of 487.3 nM AuNPs and diluted to 10 mL with 0.150 M KCl buffered to pH 7.4 with 0.01 M HEPES. These conditions were selected to reach a concentration range optimal for tracking (10⁸-10⁹ particles·mL⁻¹) [32] where the number of vesicles was determined using vesicle hydrodynamic diameters and the estimated surface area of each lipid. Samples were injected directly into the sample chamber using Luer Lok syringes (BD). Data were collected on 1 mL aliquots of this solution. Similar measurements were collected on samples of vesicles or AuNPs

alone. Analysis of the number distribution of particle sizes was conducted using NTA 3.0 software using a detection threshold of 4. The detection threshold establishes the minimum pixel brightness by the software for particle tracking, and settings were adjusted according to manufacturer recommendation to eliminate tracking background noise. The camera level setting of 13 was selected such that all particles could be clearly detected with no more than 20% of particles reaching pixel saturation. The frame rate of the camera was 22.5 - 28.1 frames per second.

2.4.2. Dynamic light scattering (DLS)

Briefly, dynamic light scattering (DLS) measures the fluctuation in the intensity of scattered light due to particles diffusion. Intensity fluctuations are converted to translational diffusion coefficients via the autocorrelation function, G(t), by cumulants analysis (a moments expansion) [33]:

$$G(t) = A[1 + B\exp(-2D_{\mathrm{T}}q^{2}\tau + \mu_{2}\tau^{2})]$$
 (2)

where A is the y-intercept of the correlation function, B is the baseline, D_T is the translational diffusion coefficient, q is the scattering vector, τ is the time delay, and μ_2 is the second moment of the cumulants expansion. Because scattering intensity is proportional to particle size, D_T is intensity (or Z)- averaged. A Z-averaged hydrodynamic diameter $d_{h,Z}$ can be calculated from D_T using the Stokes-Einstein equation. $d_{h,Z}$ is an intensity-weighted mean hydrodynamic diameter and is highly weighted towards larger particles [33]. The polydispersity index (PDI), a measure of the width of distribution of hydrodynamic diameters, is derived from μ_2 [33]. If one makes the assumption that all particles are solid spheres, a mass-averaged or number-averaged hydrodynamic diameter can be estimated from $d_{h,Z}$ and μ_2 [33].

Samples of 5 nM AuNPs, vesicles at 1 mM lipid, or a mixture of 5 nM AuNPs and vesicles at 1 mM lipid were analyzed using DLS (Malvern Zetasizer Nano ZS). A 173° backscattering angle was used, with a 633 nm He-Ne laser and temperature held at 25.0 °C. Each sample was placed in a solution of 0.150 M KCl buffered to pH 7.4 with 0.01 M HEPES. The AuNP:vesicle ratio was held at ~1:27 AuNP:vesicle ratio, the same as that used for later NTA measurements. The number of AuNPs was estimated based on their measured hydrodynamic diameter and starting concentration. Vesicle numbers were determined using lipid concentration, particle size, and estimated surface area of lipid.

2.4.3. Laser Doppler electrophoresis

Laser doppler electrophoresis was used to determine the electrophoretic mobilities of the AuNPs, the vesicles, and the vesicles mixed with AuNPs, all in 0.150 M KCl buffered to pH 7.4 with 0.01 M HEPES at 25.0 °C (Malvern Zetasizer Nano ZS). The AuNP concentration was 5 nM and that of the vesicles was 1 mM. These concentrations correspond to \sim 1:27 AuNP:vesicle ratio. The Smoluchowski equation was used to calculate ζ -potentials from the electrophoretic mobilities.

2.5. Statistical analysis of mixture distributions

We used a simulation-based finite mixture approach to estimate the proportion of particles bound at different AuNP:vesicle ratios when mixed. The distributions of nanoparticle (AuNPs) and vesicle (SUV or SUV-gA) diameters were each obtained from experimental data and binned in 10 nm intervals for subsequent analysis. Smoothing was then applied to the average sampling distribution among three replicates [34]. To apply a finite mixture approach, each particle in the mixture is assumed to belong to only one of the following particle types: nanoparticle alone, vesicle alone, or bound species (in varying AuNP:vesicle ratios). Because the total number of particle types are known, a finite mixture scenario[35] can be applied to determine the proportion of each

particle type from an observed distribution of particle sizes. Application of the finite mixture approach first involves employing a probability mass function (pmf) to describe the proportion of a particle type in the mixture where $X_1,...X_n$ represent random samples from this finite mixture. In the implementation of mixture analysis here, X_i is the observed diameter of the ith particle. We note that pmfs are used in the case that the variable can take a finite number of values. The approach can be extended to cases with continuous random variables by using a probability mass function, replacing the summation with an integration.

$$\Pr_{mix} = (X_i = x) = \phi_{mix}(x) = \sum_{j=1}^{m} \lambda_j \phi_j(x)$$
 (3)

In this approach, m is the number of particle types, x is the bin center diameter, ϕ_j and λ_j are the pmf and corresponding proportion in the mixture of the j-th particle type. The primary goals are to estimate and construct confidence intervals of the λ_j values and compare observed (experimental) and estimated (statistically modeled) pmfs in terms of fitness.

Mathematically, the complete data are $C_i = (X_i, Z_i)$, where $Z_i = (Z_{i1},...Z_{jm})$ is a single trial multinomial random variable (*m*-dimensional vector) and $Z_{ij} \in \{0,1\}$ is the random variable indicating the *i*-th particle comes from component *j*. Note, we use upper case to denote a random quantity and lower case to signify a fixed or realization of the random quantity (i.e., observed data). Since each particle in the mixture belongs to only one particle type, we define

$$\Pr(Z_{ij} = 1) = \lambda_j, \Pr(X_i = x_i \mid Z_{ij} = 1) = \phi_j(x_i), j = 1,...,m$$
 (4)

such that

$$\sum_{j=1}^{m} \Pr(Z_{ij} = 1) = \sum_{j=1}^{m} \lambda_j = 1$$
 (5)

The complete-data likelihood (assuming the ϕ_i are known) is then given by

$$\ell_{complete}(\lambda;C) = \prod_{i}^{n} \sum_{j=1}^{m} Z_{ij} \lambda_{j} \phi_{j}(X_{i}), \tag{6}$$

where $\lambda = (\lambda_1,...\lambda_m)$ and $C = \{C_i\}^n$. When the ϕ_j are known, the λ_j values can be estimated by an expectation-maximization (EM) algorithm [35]. The EM algorithm iteratively maximizes the expectation of observed log-likelihood:

$$Q(\lambda \mid \lambda^{(t)}) = E[\log \ell_{complete}(\lambda; C) \mid x, \lambda^{(t)}], \tag{7}$$

where $\lambda^{(t)}$ is the (estimated) proportion at iteration t and updates the proportion estimate by

$$\lambda^{(t+1)} = \operatorname{argmax}_{\lambda} Q(\lambda \mid \lambda^{(t)})$$
 (8)

The expectation and maximization steps can be computed, first by updating the probability that the *i*-th data point falls into the *j*-th component:

$$p_{ij}^{(t)} := \Pr_{\lambda^{(t)}} \left(Z_{ij} = 1 | X_i = x_i \right) = \frac{\lambda_j^{(t)} \phi_j(x_i)}{\sum_{k=1}^m \lambda_k^{(t)} \phi_k(x_i)} = \left[1 + \sum_{k \neq j} \frac{\lambda_k^{(t)} \phi_k(x_i)}{\lambda_j^{(t)} \phi_j(x_i)} \right]^{-1}$$
(9)

Then by calculating an estimate of λ by

$$\lambda_j^{(t+1)} = \frac{1}{n} \sum_{i}^{n} p_{ij}^{(t)}, j = 1, ..., m.$$
 (10)

The estimation process is conducted iteratively and terminated when the difference between $\lambda^{(t+1)}$ and $\lambda^{(t)}$ is sufficiently small, chosen here to be when $\sum_{j=1}^{m} |\lambda^{(t+1)} - \lambda^{(t)}| < 10^{-6}$, that is, when the change between iterations is precise to the 6^{th} decimal place. We used a self-written R code to implement this iterative finite mixture process.

A non-parametric spline[34] was applied to smooth the sample probability mass function (ϕ_j) , which consisted of a set of relative frequencies of particle diameters calculated from diffusion coefficients using one of two diffusional models (viz. the Stokes–Einstein or Kirkwood–Riseman models) [36,37]. A large number of random sampling from the relative frequencies is necessary to

simulate a probability mass function for the mixture (ϕ_{mix}). We determined that the use of 10⁶ random samples was sufficient to accurately mimic experimental mixture data. For further statistical inference, the sampling and estimation procedures are repeated 1,000 times. In sum, our approach can be viewed as a form of parametric bootstrapping [38], which can be used to recover the function of an underlying distribution.

This process can be thought of as a random drawing of particles from distributions of nanoparticle and vesicle diameters to produce an estimated mixture distribution. Particle diameters are obtained from measured diffusion coefficients by application of one of two diffusional models. The fitness of each model is assessed by measuring the statistical distance between estimated and observed mixture distributions using the Cramér–von Mises criterion, which is the sum of squared distances between the estimated and observed distribution [39]. A Wilcoxon rank sum test is used to compare the CVMs based on Stokes–Einstein or Kirkwood–Riseman model. Computations were conducted in R with packages [40], and the R code is included in the SI for user reference.

3. Results and discussion

3.1. Assessment of nanoparticle binding to vesicles by DLS

DLS data were collected for nanoparticles alone, vesicles alone, and mixtures of nanoparticles and vesicles and are reported as Z-average (intensity-weighted) and number-average hydrodynamic diameters. Vesicle hydrodynamic diameters are reported in Table 1. The vesicle sizes are larger than the 50 nm pore size as commonly observed for vesicles extruded through filter sizes <100 nm [27,41]. Because Rayleigh scattering intensity increases with the square of the mass of particles (and the sixth power of the radius of solid spherical particles), the DLS signal is more sensitive to the presence of large particles, and the Z-averaged hydrodynamic diameter d_{hZ} is the most direct measure provided by DLS. The number-average hydrodynamic diameter is calculated

from d_{hZ} by assuming that all particles are solid spheres, and is less sensitive to larger particles than the Z-average hydrodynamic diameter.

Vesicle d_{hZ} , based on the average of three replicates of a single sample, was measured as 135 nm (Table 1). Vesicle size is larger than the 50 nm pore size, a pattern that is commonly observed for vesicles extruded through filter sizes <100 nm [27,41]. Incorporation of gA did not measurably affect vesicle size (Table 1). Hydrodynamic diameters for AuNPs represent the average of three replicates of a single sample, and these data are reported in Table 1. The nanoparticle size of ~90 nm is significantly larger than that measured by UV-Vis or TEM (3.3 nm, Supplemental Information). We note that nanomaterials placed in high salt buffers aggregate significantly beyond their TEM core size, consistent with numerous other studies demonstrating aggregation of colloidal gold nanomaterials in saline media [24,42]. Measured ζ-potentials represent the average of five replicates of a single sample, and these data are reported in Table 1. As expected, zwitterionic DPhPC vesicles exhibited ζ-potentials near 0. Addition of gA did not alter vesicle ζ-potential. The AuNPs exibited negative ζ-potentials as expected.

Anionic AuNPs (~90 nm in diameter due to aggregation under our conditions, Table 1) were introduced to suspensions of vesicles (~130 nm diameter) that lacked or contained gA to determine if the inclusion of this channel-forming peptide alters nanoparticle binding. Our previous work of AuNP interactions with gA-containing lipid bilayers on flat surfaces did show that gA function was altered by AuNPs, albeit in an indirect way via AuNP perturbation of lipid bilayers rather than direct binding to gA [21]. Thus, the possibility that the presence of gA in lipid vesicles could alter AuNP binding in colloidal suspension (to lipids or to gA itself) needed to be checked. Analysis of DLS data (Table 1, Fig. 1) reveals that the Z-average hydrodynamic diameter increased upon mixing vesicles with AuNPs regardless of the absence or presence of gA. However,

the magnitude of change is larger for gA-containing vesicles, suggesting that the gA enhances binding. The number-average hydrodynamic diameter increased at a statistically significant level for only the gA-containing vesicles. Together these results suggest that although binding of nanoparticles to both vesicle types occurs (as indicated by changes in the aggregation-sensitive Z-average), the presence of gA in the vesicles increases AuNP-vesicle binding, by formation of either more vesicle-particle complexes, or by increasing the size of complexes.

DLS is an ensemble method that averages over all particles in solution and does not directly measure the number concentration of particles; therefore, the technique is not readily amenable to differentiating between these two possible explanations for the increase in mean Z-average hydrodynamic size. Because NTA counts particles and measures size on a particle-by-particle basis, the technique provides the potential opportunity to determine which of these scenarios is occurring.

3.2.1. Determination of fraction of AuNPs bound from mixture distributions and NTA

Nanoparticle tracking analysis measures diffusion coefficients of individual particles by analyzing the trajectories of scattering particles captured with a video camera. Generally speaking, NTA operates under far more dilute conditions ($\sim 10^7 - 10^9$ particles/mL) compared to DLS ($\sim 10^{14} - 10^{16}$ particles/mL). Samples of AuNPs with vesicles (alone or with gA) were prepared at $10^8 - 10^9$ particles/mL and then analyzed by NTA. Histograms of diffusion coefficients are plotted in Fig. 2. Median number-averaged hydrodynamic diameters calculated from these histograms using the Stokes-Einstein equation indicates a change upon introduction of AuNPs to gA-containing vesicles (p < 0.001; non-parametric Mann-Whitney U test), but not to vesicles lacking gA (Table 1). The observation that the presence of gA may lead to more binding of AuNPs is consistent with

the interpretation of the DLS results (*vide supra*). However, this analysis alone is insufficient to determine specific AuNP:vesicle binding ratios or quantitation of the degree of binding.

Diffusion coefficient histograms (Fig. 2) demonstrate multi-modal character for both SUV and SUV-gA samples. Cursory visual assessment of the histograms suggests that there may be shifts in individual peaks upon addition of AuNPs towards smaller diffusion coefficients (larger particle hydrodynamic diameters). However, it is not possible to confidently assign a specific peak to a particular particle type or to quantify the distribution between free and bound nanoparticles by visual examination alone.

To provide a more descriptive and quantitative measure of nanoparticle binding to vesicles lacking or containing gA, we applied statistical mixture distribution to the NTA data [43]. Fig. 3 depicts a schematic of how mixture distributions were employed. The process involves randomly drawing nanoparticle and vesicle diffusion coefficients from measured NTA histogram data, computationally "binding" them in different AuNP:vesicle ratios and calculating a diffusion coefficient from a model equation, and then repeating this process until the new histogram of computationally bound species closely matches ($\alpha = 0.05$, 1000 replicates) that which was experimentally collected.

3.2.2. Stokes-Einstein model

Application of mixture distributions to NTA data requires that model equation be applied that relates diffusion coefficients to particle binding. The Stokes–Einstein model relates the translational diffusion coefficient to particle hydrodynamic diameter (d_h) [44]:

$$d_h = \frac{k_{\rm B}T}{3\pi\eta D_{\rm T}} \tag{11}$$

where $k_{\rm B}$, T, and η are the Boltzmann constant, temperature, and solvent viscosity, respectively. We applied the Stokes–Einstein model to the experimental data by assuming that two bound

spherical particles diffuse such that their diffusion coefficient equals that of a single larger sphere of encompassing diameter (i.e., the bound pair is modeled as a sphere with diameter equal to the sum of the diameters of the two particles) For example, an 'attached' pair of one 130 nm-diameter vesicle and one 90-nm nanoparticle was assumed to diffuse with the same diffusion coefficient as one 220 nm spherical particle, while a 'bridged' complex of two vesicles and one nanoparticle is assigned the same diffusion coefficient of a 350 nm spherical particle (Figure 3C).

Figs. 4 and 5 summarize the results from application of the Stokes–Einstein model and subsequent mixture distribution analysis of NTA data. Results from this model fit all of the experimental data such that they are explained by only four possible components: AuNPs, vesicles, and bound species—either attached (1:1 AuNP:vesicle) or bridged (1:2 AuNP:vesicle). Application of this model predicts that the attached (1:1) and bridged (1:2) populations increase from ~3% to 34% and 0.1% to 0.5%, respectively, upon inclusion of gA in vesicles. This increase in binding to gA-containing vesicles qualitatively agrees with a previous study which found that AuNPs can bind to gA-containing membranes [24].

The Stokes–Einstein model assumes an effective spherical shape of AuNP–vesicle species. Since the 'attached' and 'bridged' complexes more closely resemble a linear chain, the spherical assumption will estimate a slower diffusion coefficient than the actual chain [44] [36,45],. Thus, Stokes–Einstein may fail to accurately describe the diffusion of particles that bind to form a linear chain, which may be an especially marked error for AuNP–vesicle binding that exceeds the 1:1 (attached) ratio.

3.2.3 Kirkwood–Riseman model

To better account for inaccuracies in applying the Stokes–Einstein relation to chain-like complexes, we considered the Kirkwood–Riseman model [36]. The Kirkwood–Riseman model

postulates spherical subunits binding in a linear chain and assumes that the size of each subunit is identical [36]. Although the nanoparticles and vesicles differ somewhat in size (Table 1), the Kirkwood-Riseman model was expected to provide a more accurate description than Stokes-Einstein of the diffusive properties of nanoparticle-vesicle complexes if the binding events produced linear chains .

The Kirkwood–Riseman model calculates the ratio of friction factors between chain (f) and monomer (f_m) as [36]

$$\frac{f}{f_m} = N \left[1 + \left(\frac{1}{N} \right) \sum_i \sum_{j \neq 1} \alpha_{ij}^{-1} \right]^{-1} \tag{12}$$

where N is the number of subunits in the chain and α_{ij} denotes the distance between subunits i and j. By this equation, the ratio of friction factors for a two subunit chain is 1.33 and that of a three subunit chain is 1.64. The friction factor (f) [36]:

$$f = \frac{kT}{D_T} = 3\pi \eta d_h \tag{13}$$

is related to d_h and D_T . To apply the Kirkwood–Riseman model, we assumed that the nanoparticle and vesicle hydrodynamic diameters were similar (see Table 1), and used the bin center radii from the NTA histogram and adjustment factors (e.g., $1.33 \times$ (vesicle radius) for 1:1 AuNP:vesicle bound species) to calculate attached sizes.

To assess AuNP-vesicle binding, we assumed that all binding configurations demonstrate vesicle: AuNP ratios ≥ 1 , since vesicles were present in far excess relative to nanoparticles in our NTA experiments. Moreover, we assumed that the AuNPs (already aggregated to 85 nm from their core 3.3 nm diameters) will not undergo additional aggregation in the presence of vesicles. These two assumptions taken together limit the potential binding configurations to 1:1 AuNP:vesicle (attached) and 1:2 AuNP:vesicle (bridged) populations. Application of the Kirkwood–Riseman

model in this manner reveals that attached species (1:1 AuNP:vesicle) increased from ~16% to 41% and bridged species (1:2 AuNP:vesicle) increased from 0.01% to 20% with the inclusion of gA in vesicles. Thus, application of either the Stokes-Einstein or the Kirkwood-Riseman models to the NTA data demonstrate that inclusion of gA in vesicles leads to an increase in the number of both attached (1:1) and bridged (1:2) species (Table S1). Up to ~2% (e.g., sum of Table S1 is 98.1% instead of 100%) of the experimentally measured diffusion coefficients cannot be accounted for using the Kirkwood–Riseman model when chain binding is limited to attached (1:1) and bridged (1:2) species according to the criteria we applied. The failure to capture the entire population may be attributed to the presence of a small population of species that have aggregated beyond the assigned 1:1 or 1:2 binding states.

4. Conclusion

We demonstrate that the application of statistical mixture distributions to analyze particle size distributions from NTA experiments can be used to assess binding between gold nanoparticles and lipid vesicles and provides quantitative information on the proportion of particles bound in different configurations. Employing two different diffusion models, Stokes–Einstein and Kirkwood–Riseman, demonstrated that the proportion of binding in different ratios is sensitive to model type. The fitness of each model was tested using the Cramér–von Mises criterion, or the sum of squared distances between the estimated and observed distribution resulting from statistical analysis, and the Kirkwood–Riseman was determined to be the more favorable of the two models. The Kirkwood–Riseman model may serve as a better physical model for the proposed AuNP–vesicle binding scenarios illustrated in Figure 3C. Thus, model choice is an important consideration when applying mixture distributions to NTA data sets, and both the underlying assumptions of each model and model fitness should be carefully considered. By the Kirkwood–

Riseman model, the presence of gA peptide was found to increase total binding by approximately 4-fold due to increases in both the attached (1:1 AuNP:Vesicle) and bridged (1:2 AuNP:Vesicle) binding configurations. The application of mixture distributions to NTA analysis can thus provide a quantitative description about proportion bound in varying particle binding configurations. In addition, the results described here provide clear hypotheses to test for NP-liposome-protein interactions, that could be interrogated by a number of orthogonal experiments, such as fluorescence resonance energy transfer experiments between labeled species, or cryo-electron microscopy.

CRediT authorship contribution statement

Isabel U. Foreman-Ortiz: Conceptualization, Methodology, Formal Analysis, Investigation, Writing - original draft, Visualization. Ting Fung Ma: Methodology, Software, Formal Analysis, Writing - original draft. Brandon M. Hoover: Investigation, Writing - original draft. Meng Wu: Resources, Writing - original draft. Catherine J. Murphy: Resources, Reviewed manuscript. Writing - Review and editing manuscript. Regina M. Murphy: Methodology, Resources, Reviewed manuscript. Joel A. Pedersen: Conceptualization, Writing - Review & editing manuscript, Supervision.

Declaration of competing interest

The authors declare no competing financial interest.

Acknowledgements

This work was supported by the National Science Foundation under the NSF Center for Sustainable Nanotechnology (CHE-2001611), CBET-1703237, and the William F. Vilas Trust of the University of Wisconsin. J.A.P. acknowledges support from a Vilas Distinguished Achievement Professorship. We thank Jingyi Huang for helpful comments on an earlier version of this manuscript.

Appendix A. Supplementary Data

References

- [1] A.E. James, J.D. Driskell, Monitoring gold nanoparticle conjugation and analysis of biomolecular binding with nanoparticle tracking analysis (NTA) and dynamic light scattering (DLS), Analyst. 138 (2013) 1212–1218. https://doi.org/10.1039/c2an36467k.
- [2] A. Kim, W.B. Ng, W. Bernt, N.J. Cho, Validation of Size Estimation of Nanoparticle Tracking Analysis on Polydisperse Macromolecule Assembly, Sci. Rep. 9 (2019) 1–14. https://doi.org/10.1038/s41598-019-38915-x.
- [3] D. Yang, X. Lu, Y. Fan, R.M. Murphy, Evaluation of Nanoparticle Tracking for Characterization of Fibrillar Protein Aggregates, AIChE. 60 (2014) 1236–1244. https://doi.org/10.1002/aic.
- [4] V. Filipe, A. Hawe, W. Jiskoot, Critical evaluation of nanoparticle tracking analysis (NTA) by NanoSight for the measurement of nanoparticles and protein aggregates, Pharm. Res. 27 (2010) 796–810. https://doi.org/10.1007/s11095-010-0073-2.
- [5] R.A. Dragovic, C. Gardiner, A.S. Brooks, D.S. Tannetta, D.J.P. Ferguson, P. Hole, B. Carr, C.W.G. Redman, A.L. Harris, P.J. Dobson, P. Harrison, I.L. Sargent, Sizing and phenotyping of cellular vesicles using Nanoparticle Tracking Analysis, Nanomedicine Nanotechnology, Biol. Med. 7 (2011) 780–788. https://doi.org/10.1016/j.nano.2011.04.003.
- [6] N.C. Bell, C. Minelli, J. Tompkins, M.M. Stevens, A.G. Shard, Emerging techniques for submicrometer particle sizing applied to stöber silica, Langmuir. 28 (2012) 10860–10872. https://doi.org/10.1021/la301351k.
- [7] N. Sanchez, D. Soulet, E. Bonnet, F. Guinchard, S. Marco, E. Vetter, N. Nougarede, Rabies Vaccine Characterization by Nanoparticle Tracking Analysis, Sci. Rep. 10 (2020) 1–8. https://doi.org/10.1038/s41598-020-64572-6.
- [8] V. Kestens, V. Bozatzidis, P.J. De Temmerman, Y. Ramaye, G. Roebben, Validation of a particle tracking analysis method for the size determination of nano- and microparticles, J. Nanoparticle Res. 19 (2017). https://doi.org/10.1007/s11051-017-3966-8.
- [9] E. van der Pol, F.A.W. Coumans, A.E. Grootemaat, C. Gardiner, I.L. Sargent, P. Harrison, A. Sturk, T.G. van Leeuwen, R. Nieuwland, Particle size distribution of exosomes and microvesicles determined by transmission electron microscopy, flow cytometry, nanoparticle tracking analysis, and resistive pulse sensing, J. Thromb. Haemost. 12 (2014) 1182–1192. https://doi.org/10.1111/jth.12602.
- [10] B. Wang, L. Zhang, C.B. Sung, S. Granick, Nanoparticle-induced surface reconstruction of phospholipid membranes, Proc. Natl. Acad. Sci. U. S. A. 105 (2008) 18171–18175. https://doi.org/10.1073/pnas.0807296105.
- [11] B.Y. Moghadam, W.-C. Hou, C. Corredor, P. Westerhoff, J.D. Posner, The role of nanoparticle surface functionality in the disruption of model cell membranes, Langmuir. 28 (2012) 16318–16326. https://doi.org/10.1038/jid.2014.371.
- [12] A. Akbarzadeh, R. Rezaei-Sadabady, S. Davaran, S.W. Joo, N. Zarghami, Y. Hanifehpour, M. Samiei, M. Kouhi, K. Nejati-Koshki, Liposome: Classification, preparation, and applications, Nanoscale Res. Lett. 8 (2013) 1–8. https://doi.org/10.1186/1556-276X-8-102.
- [13] E. Rideau, R. Dimova, P. Schwille, F.R. Wurm, K. Landfester, Liposomes and polymersomes: a comparative review towards cell mimicking, Chem. Soc. Rev. 47 (2018)

- 8572-8610. https://doi.org/10.1039/c8cs00162f.
- [14] L.-C. Cheng, X. Jiang, J. Wang, C. Chen, R.-S. Liu, Nano-bio effects: interaction of nanomaterials with cells., Nanoscale. 5 (2013) 3547–69. https://doi.org/10.1039/c3nr34276j.
- [15] S. Dante, A. Petrelli, E.M. Petrini, R. Marotta, A. Maccione, A. Alabastri, A. Quarta, F. De Donato, T. Ravasenga, A. Sathya, R. Cingolani, R. Proietti Zaccaria, L. Berdondini, A. Barberis, T. Pellegrino, Selective targeting of neurons with inorganic nanoparticles: Revealing the crucial role of nanoparticle surface charge, ACS Nano. 11 (2017) 6630–6640. https://doi.org/10.1021/acsnano.7b00397.
- [16] C.L. Ventola, D.J. Bharali, S.A. Mousa, The Nanomedicine Revolution: Part 1: Emerging Concepts. Pharmacy and Therapeutics., Pharmacol. Ther. 128 (2010) 512–525. https://doi.org/10.1016/j.pharmthera.2010.07.007.
- [17] W. Jiang, K. Yang, R.W. Vachet, B. Xing, Interaction between oxide nanoparticles and biomolecules of the bacterial cell envelope as examined by infrared spectroscopy, Langmuir. 26 (2010) 18071–18077. https://doi.org/10.1021/la103738e.
- [18] J. Bozich, M. Hang, R.J. Hamers, R. Klaper, Core chemistry influences the toxicity of multicomponent metal oxide nanomaterials, lithium nickel manganese cobalt oxide, and lithium cobalt oxide to Daphnia magna, Environ. Toxicol. Chem. 36 (2017) 2493–2502.
- [19] M.A. Maurer-Jones, I.L. Gunsolus, C.J. Murphy, C.L. Haynes, Toxicity of engineered nanoparticles in the environment, Anal. Chem. 85 (2013) 3036–3049. https://doi.org/10.1021/ac303636s.
- [20] A.E. Nel, L. Mädler, D. Velegol, T. Xia, E.M. V Hoek, P. Somasundaran, F. Klaessig, V. Castranova, M. Thompson, Understanding biophysicochemical interactions at the nanobio interface, Nat. Mater. 8 (2009) 543–557. https://doi.org/10.1038/nmat2442.
- [21] C. Montis, D. Maiolo, I. Alessandri, P. Bergese, D. Berti, Interaction of nanoparticles with lipid membranes: A multiscale perspective, Nanoscale. 6 (2014) 6452–6457. https://doi.org/10.1039/c4nr00838c.
- [22] C. Montis, L. Caselli, F. Valle, A. Zendrini, F. Carlà, R. Schweins, M. Maccarini, P. Bergese, D. Berti, Shedding light on membrane-templated clustering of gold nanoparticles, J. Colloid Interface Sci. 573 (2020) 204–214. https://doi.org/10.1016/j.jcis.2020.03.123.
- [23] J. Liu, Xiuru; Li, Xiaoqiu; Xu, Wu; Zhang, Xiaohan; Huang, Zhicheng; Wang, Feng; Liu, Sub-Angstrom Gold Nanoparticle and Liposome Interfaces Controlled by Halides, Langmuir. 34 (2018) 6628–6635. https://doi.org/10.1021/acs.langmuir.8b01138.
- [24] I.U. Foreman-Ortiz, D. Liang, E.D. Laudadio, J.D. Calderin, M. Wu, P. Keshri, X. Zhang, M.P. Schwartz, R.J. Hamers, V.M. Rotello, C.J. Murphy, Q. Cui, J.A. Pedersen, Anionic nanoparticle-induced perturbation to phospholipid membranes affects ion channel function, Proc. Natl. Acad. Sci. U. S. A. 117 (2020) 27854–27861. https://doi.org/10.1073/pnas.2004736117.
- [25] J.S. Bozich, S.E. Lohse, M.D. Torelli, C.J. Murphy, R.J. Hamers, R.D. Klaper, Surface chemistry, charge and ligand type impact the toxicity of gold nanoparticles to *Daphnia magna*, Environ. Sci. Nano. 1 (2014) 260–270. https://doi.org/10.1039/C4EN00006D.
- [26] W. Haiss, N.T.K. Thanh, J. Aveyard, D.G. Fernig, Determination of size and concentration of gold nanoparticles from UV-Vis spectra, Anal. Chem. 79 (2007) 4215–4221. https://doi.org/10.1021/ac0702084.
- [27] L.D. Mayer, M.J. Hope, P.R. Cullis, Vesicles of variable sizes produced by a rapid

- extrusion procedure, BBA Biomembr. 858 (1986) 161–168. https://doi.org/10.1016/0005-2736(86)90302-0.
- [28] E. S. Melby, C. Allen, I. U. Foreman-Ortiz, E. R. Caudill, T. R. Kuech, A. M. Vartanian, X. Zhang, C. J. Murphy, R. Hernandez, J. A. Pedersen, Peripheral membrane proteins facilitate nanoparticle binding at lipid bilayer interfaces, Langmuir. 34 (2018) 10793–10805. https://doi.org/10.1021/acs.langmuir.8b02060.
- [29] A. Chattopadhyay, S.S. Rawat, D. V. Greathouse, D.A. Kelkar, R.E. Koeppe, Role of tryptophan residues in gramicidin channel organization and function, Biophys. J. 95 (2008) 166–175. https://doi.org/10.1529/biophysj.107.124206.
- [30] S.S. Rawat, D.A. Kelkar, A. Chattopadhyay, Monitoring gramicidin conformations in membranes: A fluorescence approach, Biophys. J. 87 (2004) 831–843. https://doi.org/10.1529/biophysj.104.041715.
- [31] J.A. Gallego-Urrea, J. Tuoriniemi, M. Hassellöv, Applications of particle-tracking analysis to the determination of size distributions and concentrations of nanoparticles in environmental, biological and food samples, TrAC Trends Anal. Chem. 30 (2011) 473–483. https://doi.org/10.1016/j.trac.2011.01.005.
- [32] B.M. Hoover, R.M. Murphy, Evaluation of Nanoparticle Tracking Analysis for the Detection of Rod-Shaped Particles and Protein Aggregates, J. Pharm. Sci. 109 (2019) 452–463. https://doi.org/10.1016/j.xphs.2019.10.006.
- [33] J. Stetefeld, S.A. McKenna, T.R. Patel, Dynamic light scattering: a practical guide and applications in biomedical sciences, Biophys. Rev. 8 (2016) 409–427. https://doi.org/10.1007/s12551-016-0218-6.
- [34] C. Gu, Smoothing spline ANOVA models: R package gss, J. Stat. Softw. 58 (2014) 1–25. https://doi.org/10.18637/jss.v058.i05.
- [35] A.P. Dempster, N.M. Laird, D.B. Rubin, Maximum Likelihood from Incomplete Data via the EM Algorithm, J. R. Stat. Soc. Ser. B. 39 (1977) 1–38.
- [36] J.G. Kirkwood, J. Riseman, The intrinsic viscosities and diffusion constants of flexible macromolecules in solution, J. Chem. Phys. 16 (1948) 565–573. https://doi.org/10.1063/1.1746947.
- [37] J.T. Edward, Molecular volumes and the Stokes-Einstein equation, J. Chem. Educ. 47 (1970) 261–270. https://doi.org/10.1021/ed047p261.
- [38] B. Efron, R.J. Tibshirani, An Introduction to the Bootstrap, Chapman and Hall, 1993.
- [39] R.B. D'Agostino, M.A. Stephens, Goodness-of-fit-techniques, in: Chapter 4, 1986: pp. 97–193.
- [40] R Core Team, R: A language and environment for statistical computing, (2018).
- [41] D.G. Hunter, B.J. Frisken, Effect of extrusion pressure and lipid properties on the size and polydispersity of lipid vesicles, Biophys. J. 74 (1998) 2996–3002. https://doi.org/10.1016/S0006-3495(98)78006-3.
- [42] R. Pamies, J.G.H. Cifre, V.F. Espín, M. Collado-González, F.G.D. Baños, J.G. De La Torre, Aggregation behaviour of gold nanoparticles in saline aqueous media, J. Nanoparticle Res. 16 (2014). https://doi.org/10.1007/s11051-014-2376-4.
- [43] A.P. Dempster, N.M. Laird, D.B. Rubin, Maximum Likelihood from Incomplete Data Via the EM Algorithm, 1977. https://doi.org/10.1111/j.2517-6161.1977.tb01600.x.
- [44] R. Evans, G. Dal Poggetto, M. Nilsson, G.A. Morris, Improving the Interpretation of Small Molecule Diffusion Coefficients, Anal. Chem. 90 (2018) 3987–3994. https://doi.org/10.1021/acs.analchem.7b05032.

[45] R. Stepto, Interpretation of the effects of segmental friction on the diffusion coefficients of polymer chains, Die Makromol. Chemie. 190 (1989) 549–557. https://doi.org/10.1002/macp.1989.021900311.

Table 1. Hydrodynamic and electrokinetic properties of the gold nanoparticles (AuNPs) and lipid vesicles.^a

| | Hydrodynamic Diameter (nm) | | | 0 | |
|----------------|----------------------------|----------------|------------------|----------------|-----------------|
| | Dynamic Light Scattering | | | NTA | ζ-Potential |
| Sample | Z-average | Number-average | PDI ^b | Number-average | (mV) |
| AuNPs | 90 ± 14 | 60 ± 17 | 0.22 ± 0.01 | 83 ± 1.5 | -25.0 ± 1.4 |
| SUV | 135 ± 0.9 | 90 ± 10 | 0.12 ± 0.01 | 112 ± 1.9 | -3.0 ± 0.9 |
| SUV + AuNPs | 156 ± 1.0 | 97 ± 9.4 | 0.20 ± 0.01 | 114 ± 5.0 | -2.1 ± 0.6 |
| SUV-gA | 129 ± 1.2 | 78 ± 8.3 | 0.17 ± 0.01 | 120 ± 36 | -3.6 ± 0.7 |
| SUV-gA + AuNPs | 189 ± 4.9 | 120 ± 18 | 0.23 ± 0.01 | 150 ± 54 | -3.3 ± 0.2 |

^a Values presented as a mean \pm for three replicates of a single sample. The stoichiometry of the AuNP:vesicle mixtures are 1:27.

^b Polydispersity Index (PDI), a measure of heterogeneity in hydrodynamic diameters.

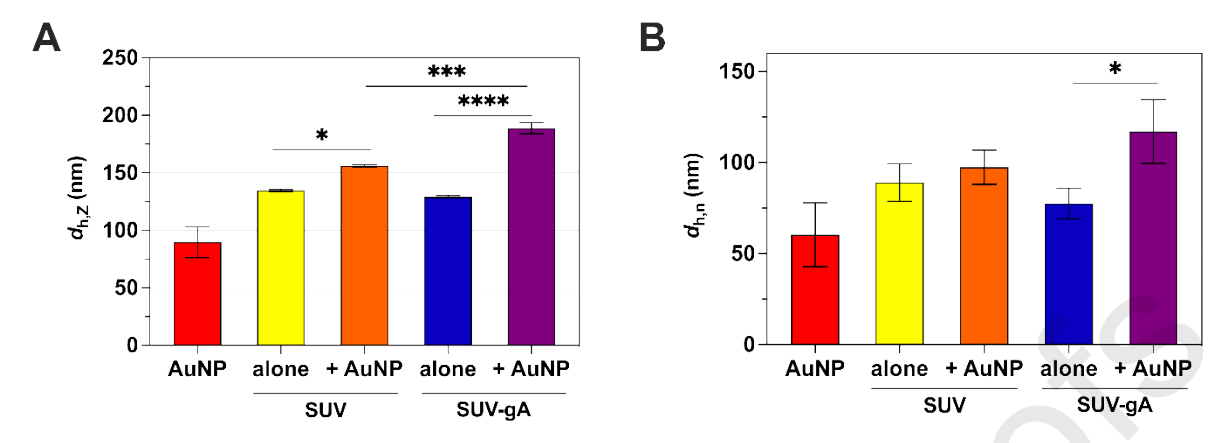


Figure 1. Average hydrodynamic diameters (d_h) of AuNPs, DPhPC vesicles (SUV alone or incorporating gramicidin A (SUV-gA), and AuNPs interacting with vesicles as determined by dynamic light scattering (DLS). (A) Z-average hydrodynamic diameter $(d_{h,Z})$ indicating that anionic AuNPs bind to vesicles both lacking and containing gA. (B) Number-average diameter $(d_{h,n})$ showing a size change (p < 0.05) resulting only from interaction of AuNPs with gA-containing vesicles

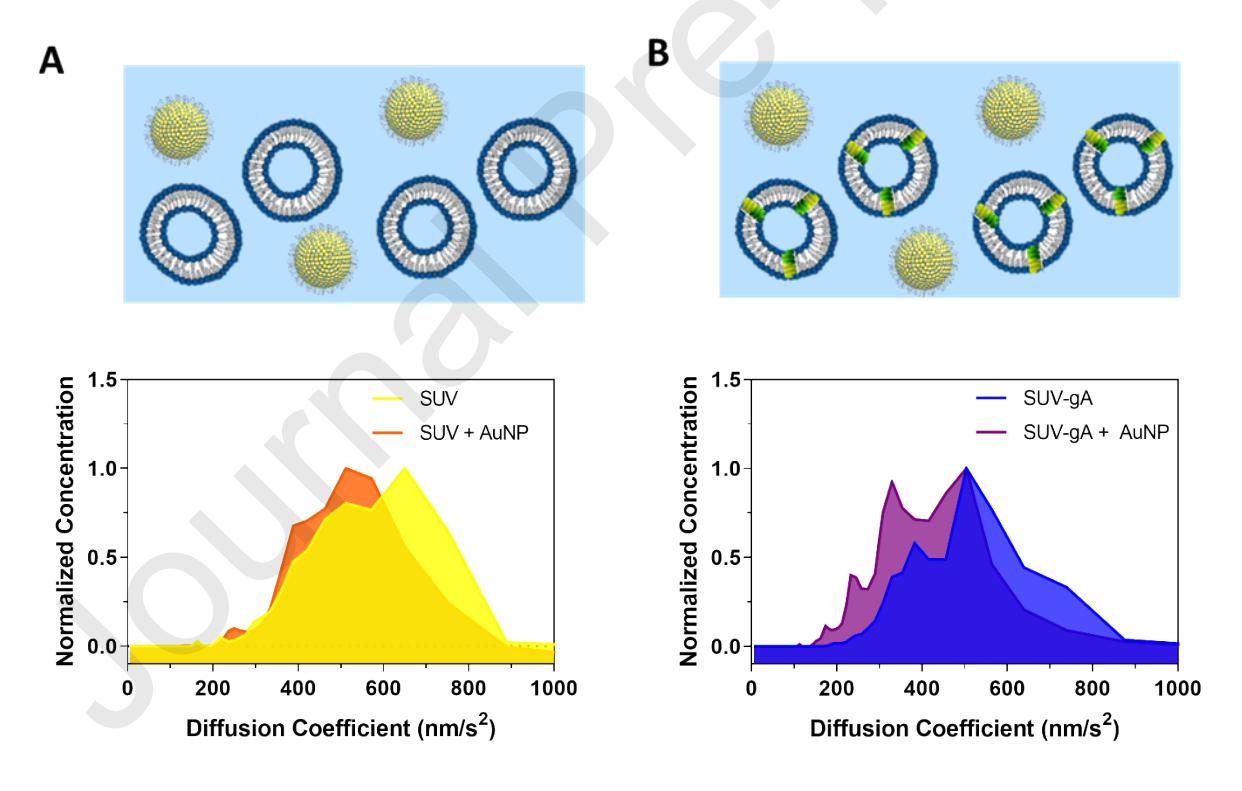


Figure 2. Representative histograms of particle diffusion coefficients measured by NTA for a single replicate of each sample, normalized to maximum particle number concentration. (A) DPhPC SUVs with and without addition of AuNPs and (B) SUV-gA with and without addition of AuNPs, both showing decreases in diffusion coefficients upon addition of AuNPs that justify further, more detailed analysis of NTA data.

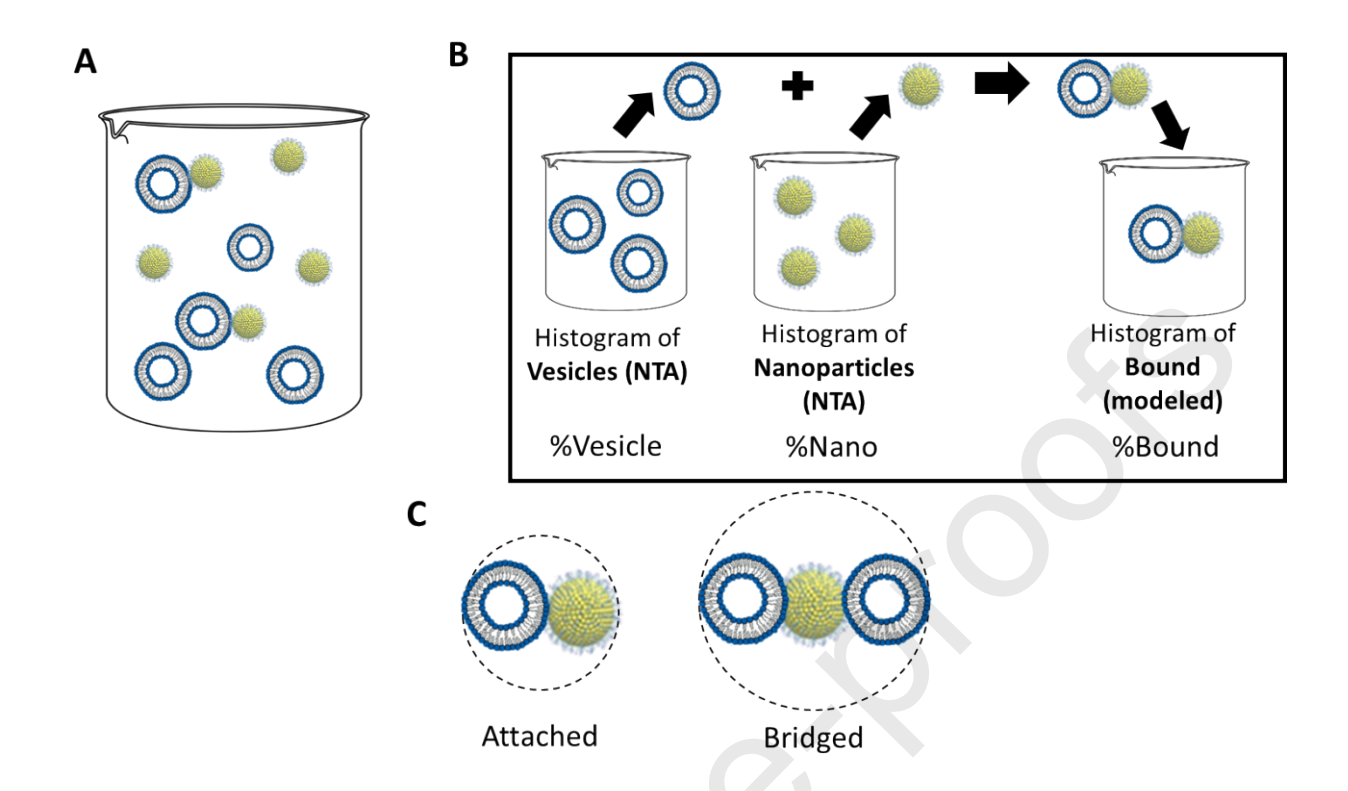


Figure 3. Schematic depicting the concept of mixture distributions as applied to a nanoparticle-vesicle system where (A) vesicles, nanoparticles, and bound AuNP-vesicle species all exist in solution and (B) mixture distribution analysis is applied by drawing vesicle and nanoparticle sizes from NTA measurements, and AuNP-vesicle bound species are artificially formed using either the Stokes-Einstein (SE) or Kirkwood-Riseman (KR) models to generate a third modeled histogram of bound species that closely matches the measured histogram for AuNP + vesicle. Two possible binding scenarios and their SE hydration spheres are depicted in (C) a 1:1 AuNP:Vesicle ratio or a 1:2 AuNP:Vesicle ratio based on the excess of vesicles present in solution relative to the AuNP concentration.

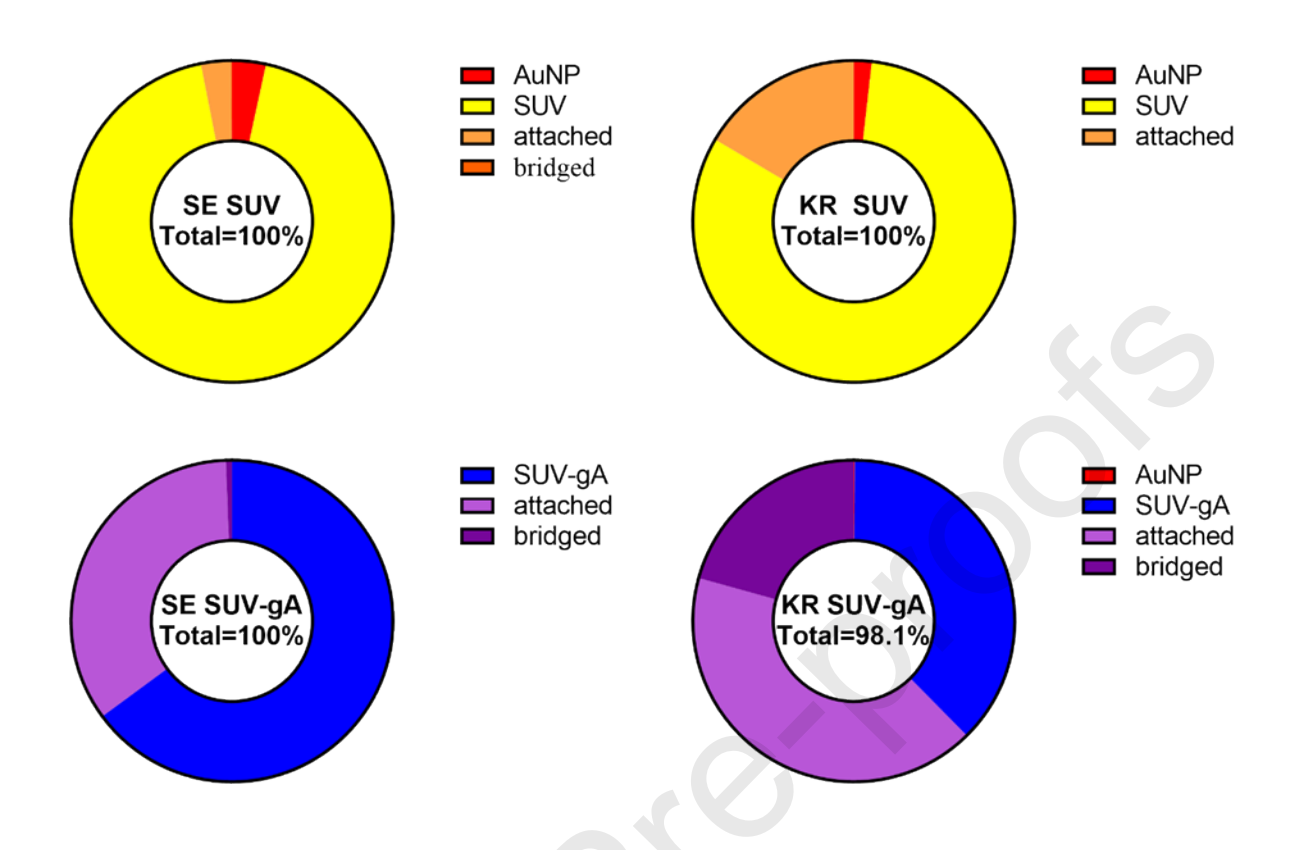


Figure 4. Comparison of gold nanoparticle (AuNP)–small unilamellar vesicle (SUV) binding using the (A, C) Stokes–Einstein (SE) and (B, D) Kirkwood–Riseman (KR) models for (A, B) SUVs and (C, D) vesicles containing gramicidin A (SUV-gA), where "attached" indicates 1:1 AuNP:vesicle and "bridged" denotes 1:2 AuNP:vesicle binding ratios. Percentages denoted in the middle of each chart indicate the percent of the measured population explained by each analysis (e.g., KR analysis of SUV-gA population accounts for 98.1% of the measured species).

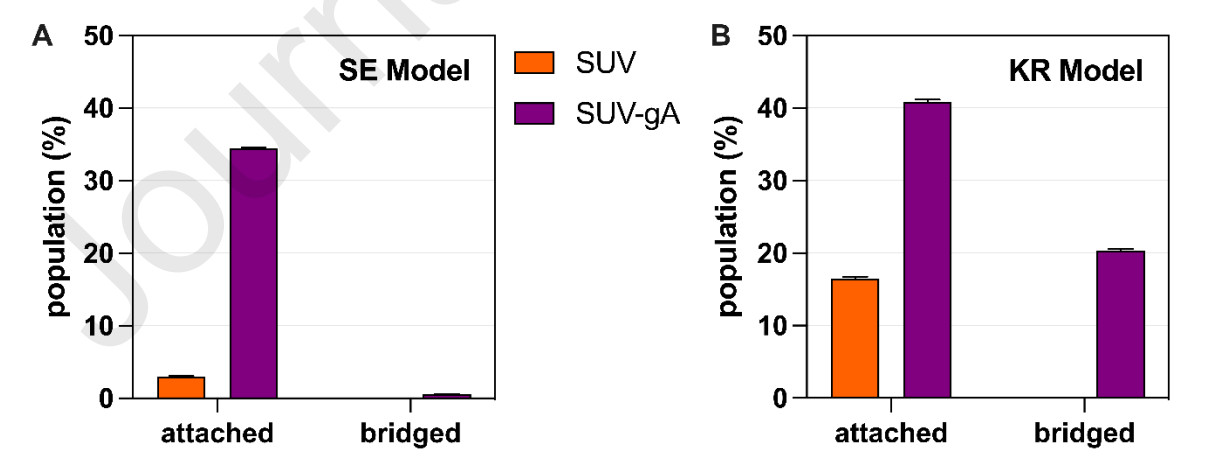


Figure 5. Population of attached (1:1 AuNP:vesicle) versus bridged (1:2 AuNP:vesicle) species based on application of the (A) Stokes–Einstein (SE) or (B) Kirkwood–Riseman (KR) model in

the statistical mixture distribution analysis of NTA data. Bars represent mean values calculated at the 95% confidence interval; error bars represent upper and lower bounds.

Declaration of competing interest

The authors declare no competing financial interest.